Renewable and Sustainable Energy Reviews 33 (2014) 499–508

Contents lists available at ScienceDirect

Renewable and Sustainable Energy Reviews

journal homepage: www.elsevier.com/locate/rser

Review of fluid dynamics aspects of Savonius-rotor-based vertical-axis wind rotors

Can Kang [a,b,*], Haixia Liu [c], Xin Yang [a]

[a] School of Energy and Power Engineering, Jiangsu University, Zhenjiang 212013, China
[b] St. Anthony Falls Laboratory, University of Minnesota, Minneapolis 55414, USA
[c] School of Material Science and Engineering, Jiangsu University, Zhenjiang 212013, China

ARTICLE INFO

Article history:
Received 14 June 2013
Received in revised form
24 January 2014
Accepted 15 February 2014
Available online 7 March 2014

Keywords:
Savonius wind rotor
Flow pattern
Rotor shape
Aerodynamic force
Shaft torque
Tip-speed ratio

ABSTRACT

The Savonius wind turbine bears unique features in both aspects of rotor structure and torque production. Continual improvement of the Savonius wind turbine motivates the authors of this review to gather, classify and discuss the quintessential parts of the relevant studies. Unambiguous priority is granted to the turbulent flow surrounding the Savonius wind rotor. Flow patterns near the Savonius wind rotor are represented with distributions of static pressure near conventional and spiral Savonius wind rotors. Assorted geometric shapes of Savonius wind rotors are demonstrated to illuminate a panorama of the development of the Savonius wind rotor, as well as to highlight the connection between rotor-based solid boundary and flow structures near Savonius wind rotor blades. Limitations of existing analytical methods used to predict the performance of the Savonius wind rotor are interpreted. Advantages of both numerical and experimental techniques in acquiring aerodynamics forces, shaft torque and internal stress distribution for the Savonius wind rotor blade are enumerated, and the difficulties incurred by curved blades and the rotation of the rotor are analyzed as well. Optimal values of tip-speed ratio corresponding to maximum power coefficient or maximum torque coefficient are different for various geometric shapes of Savonius wind rotors, which sheds new light upon the relationship between flow characteristics and performance parameters associated with the Savonius wind rotor.

Contents

* Corresponding author at: St. Anthony Falls Laboratory, University of Minnesota, Minneapolis 55414, USA.
E-mail address: kangx603@umn.edu (C. Kang).

http://dx.doi.org/10.1016/j.rser.2014.02.011
1364-0321

1. Introduction

Numerous studies of the vertical-axis wind turbine (VAWT) were carried out based upon the Savonius wind turbine invented in 1922. In recent years, the combination of theoretical, experimental and simulation achievements has significantly extended the original concept of the Savonius wind turbine [1]. Meanwhile, enriched knowledge of the Savonius wind turbine has consistently facilitated the implementation of many fresh research schemes. For instance, a Savonius hydraulic rotor, which inherited primary geometric characteristics from the conventional Savonius wind rotor, passed successfully both model experiment and in-situ performance test [2].

Continuous interaction between ambient air and wind rotor blades plays a pivotal part in the conversion from wind energy to electricity or available driving force. Such an interaction becomes perceivable with the assistance of simulation and measurement techniques. Many current studies are dedicated to describing quantitatively the relationship between flow characteristics and wind rotor performance. From the perspective of artificially controlling ambient air flow, it is tempting to devise a reliable technique for improving the quality of upstream air flow. Nevertheless, the efforts for this purpose have rarely yielded noticeable advancement, particularly on the part of large-scale wind turbines. In relevant treatises, upstream air flow is overwhelmingly assumed to be uniform and steady. By contrast, most air flows facing the wind turbines in service are three-dimensional and unsteady turbulent flows. It is widely recognized that adverse flow situations contribute considerably to the deformation of wind rotor blades and even the vibration of supporting towers.

The conventional Savonius wind rotor, featured by two semicircular blades, is simple in both appearance and aerodynamic performance, while the complexity of the curved-blade Savonius wind rotor hinges upon the solid-boundary-related turbulent flows. The replacement of straight rotor blades by curved rotor blades is advantageous, as has been corroborated by accordingly improved flow patterns and suppressed aerodynamics force fluctuations [3–5]. Meanwhile, the family of Savonius wind rotors has been constantly refreshed with new members such as two- and three-stage Savonius wind rotors. In this connection, the viewpoint that the multistage Savonius wind rotor is merely a physical superposition of individual rotors should be overturned in view of the complex impact exerted by staggered rotors on the whole wind turbine, and this impact has not been elucidated hitherto [6]·[7].

More emphasis in this review is placed upon the flow-related issues associated with the Savonius wind rotor. Besides an exemplification of practical upstream air flow, distributions of primary flow parameters near the Savonius wind rotor are illustrated and further compared with the flow field around a Darrieus wind turbine rotor. The evolution of geometric shape of the Savonius wind rotor is another prioritized subject. And various geometric shapes, as well as the adjunct devices which also lend their support to the performance improvement of the rotor, are presented. Both merits of curved blades and relevant research difficulties are detailed in three aspects, spatial flow pattern, multidirectional aerodynamics force and shaft torque. As for the prediction of the performance of the Savonius wind rotor, an objective and comprehensive discussion covers limitations of analytical models, the versatility of numerical simulation, and the pros and cons of measurement techniques. Various values of optimal tip-speed ratio are extracted from representative treatises to draw further attention to the relationship between typical flow structures and operation parameters related to the Savonius wind rotor. In addition, the impetus behind this review is also boosted by those research techniques which have facilitated studies of the Savonius wind rotor.

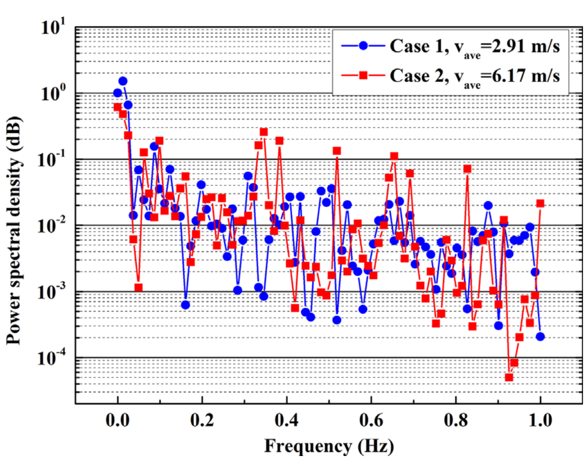


Fig. 1. Power spectral density of upstream air velocity. The sampling position was 6.0 m above local ground and 8.0 m in horizontal distance from the nearest wind turbine. The two datasets were acquired in the same duration of 75 s but on different days.

2. Turbulent flow characteristics

2.1. Upstream air flow

Atmospheric air flow is inherently turbulent, irrespective of the fact that the search of an analytical solution to the Navier–Stokes equations has been rather frustrating. Therefore, all wind rotors in operation are subject to the immediate impact of turbulent fluctuations. In turn, wind rotors act as obstacles in the presence of upstream air flow. To demonstrate velocity fluctuations in low-velocity upstream air flow, instantaneous air velocity was measured using a well-calibrated hot-wire anemometer, and the measurement was performed in a wind turbine test field situated in eastern China. This test field is exclusively suitable for testing small- and medium-size wind turbines. Two cases are individually described with the power spectral density of upstream air velocity, as shown in Fig. 1.

Both the cases shown in Fig. 1 are low-velocity cases, but the discrepancy between them is evident. As for Case 1, velocity values range from 1.22 to 3.75 m/s and the resultant time-averaged velocity v_{ave} is 2.91 m/s. Case 2 involves the velocity values varying from 4.18 to 8.36 m/s and a corresponding v_{ave} of 6.07 m/s. It is apparent that practical fluctuations of power spectral density are distinct from those hypotheses dominated by steady upstream air flow. Meanwhile, Case 2 involves protruding spikes of high power spectral density, which imply the existence of large magnitudes of kinetic energy at certain frequencies. In principle, the fluctuating situation tends to be exacerbated with the increase of time-

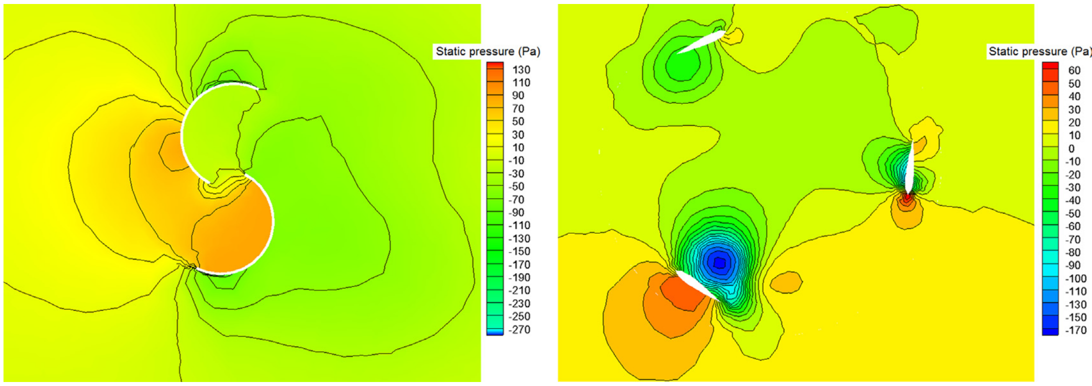


Fig. 2. Static pressure distributions near Savonius and Darrieus wind rotors. In (a), the Savonius wind rotor rotates anticlockwise, while the Darrieus wind rotor shown in (b) rotates clockwise. Identical upstream air flow conditions are imposed on the two flow fields and both the main streams flow from left to right.

averaged velocity. From another perspective, velocity fluctuations at low air velocities are conducive to the startup of wind turbines, as is particularly significant for the Savonius wind rotor, which is reputable for its good startup capability [8]. Incidentally, many Savonius wind rotors mounted on flat roofs of tall buildings suffer from adverse impacts of boundary layer. In this context, upstream air flows approaching these rotors are non-uniform along the direction parallel to rotor axes, and a low level of velocity fluctuation can impair the normal operation of these rotors and even result in the deformation of rotor shafts.

2.2. Static pressure distribution around wind rotors

Among vertical-axis wind rotors, the Savonius wind rotor possesses an unparalleled capability of producing large shaft torque. Fundamentally, shaft torque is dependent on aerodynamic forces acting upon rotor blades; the formation of these aerodynamic forces is an intricate process, which can be appreciated through a comparison between a Savonius wind rotor and a Darrieus wind rotor [9]. In general, static pressure distribution is relied upon to illustrate the evolution of aerodynamic force, and the momentum behind the rotation of a wind rotor can also be explained through examining static pressure distributions close to the two sides of each rotor blade. Here, Fig. 2(a) and (b) display cross-sectional distributions of static pressure near a conventional Savonius wind rotor and a straight-blade Darrieus wind rotor, respectively.

As shown in Fig. 2(a) and (b), the Savonius wind rotor is superior to the Darrieus wind rotor in terms of rotor solidity; therefore, the Savonius wind rotor acts as a more influential obstacle to air flow, even though the gap between the two blades forms a narrow flow passage, which accommodates merely a small portion of air flow. Another difference surfaces with a scrutinization of the situations near the two types of rotor blades. As for the Savonius wind rotor, the driving force for the rotation of the rotor rests clearly upon large-scale flow structures near the rotor blades. By contrast, the three blades of the Darrieus wind rotor are separately surrounded by three sub-areas which are unanimously marked by remarkable pressure difference. And the three sub-areas are segregated from each other, as partially weakens the collective contribution of pressure difference.

The two wind rotors shown in Fig. 2 share the geometric uniformity along rotor axis, which supports the assumption of two-dimensional flow. By contrast, curved-blade wind rotors are accompanied by complex three-dimensional flow fields, which cannot be projected onto any single cross-sectional view [3]·[5].

Hitherto, the parametric design of the Savonius wind rotor is still far from success. As a rule, the determination of primary geometric parameters depends largely upon empirical formulae,

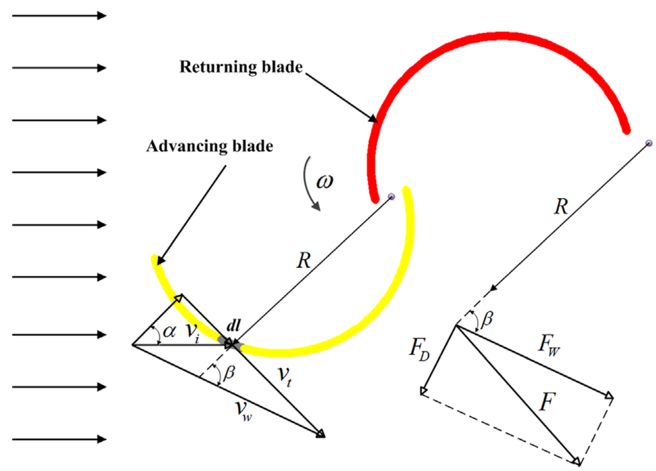


Fig. 3. Decomposition of both velocity and force on a cross section of a conventional Savonius wind rotor. Upstream air flow is uniform and moves from left to right.

which surely overloads relevant research. For instance, given that several rotor diameters are to be evaluated through a numerical technique, a complete numerical procedure has to be practiced for each scheme of rotor diameter and then several flow fields will be obtained thereby. More time-consuming is flow field analysis, through which it is anticipated to pinpoint typical flow structures near rotor blades, as well as to interpret the discrepancy among various schemes and single out the optimal scheme. In this context, a similarity law allowing for the real-time interaction between geometric parameters and flow parameters will be remarkably admirable.

3. Analytical models for the Savonius wind rotor

The momentum model is of significant importance in the early stage of the development process of wind turbines. Even in today's view, the momentum model still serves as a foundation for some new methods devised to assess the operation capability of wind rotors. The streamtube model, which is developed based upon Glauert's blade element momentum theory, is a momentum model which has proven to be successful in the study of Darrieus wind rotors [10]. Meanwhile, the streamtube model has been claimed to be theoretically feasible for the wind rotors with low tip-speed ratio. However, the exercise of the streamtube model in the study of Savonius wind rotors has not produced promising results. In this connection, it has been argued in [11] and [12] that

the main drawback of the streamtube model lies in that it is invalid in the presence of high wind rotor solidity.

Recently, owing to their insensibility to wind direction, curved-blade Savonius wind rotors have attracted much attention. As for the curved-blade Savonius wind rotor, the inapplicability of the streamtube model is more explicit. Firstly, cross sections of the curved-blade Savonius wind rotor are circumferentially staggered relative to each other, as excludes the possibility of representing the entire flow field with any isolated cross-sectional flow pattern. Secondly, the theoretical derivation of the resultant aerodynamic force acting on each curved blade based upon scattered forces acting on individual cross sections is confronted with enormous difficulties. In this context, efforts are necessitated for developing an analytical model appropriate for the Savonius wind rotor. A velocity-decomposition method fundamental for rotary hydraulic machinery is expected to be helpful for the conventional Savonius wind rotor. Rather than the whole rotor, a single blade will be treated in accordance with this method. Thus the relationship among upstream air velocity, velocity components of a rotating Savonius wind rotor blade and component forces acting upon the blade will be obtained. Such a method is schematically explained in Fig. 3.

In Fig. 3, the rotational speed ω of two identical semi-circle blades is predetermined and kept invariant. With respect to the advancing blade, a blade element with a circumferential length of dl is specified as the differential element. R is the radius of the blades. The relationship among the velocities involved is expressed by

$$\vec{v}_w = \vec{v}_i \cos\alpha + \vec{v}_t \tag{1}$$

and

$$v_t = v_i \sin\alpha + \omega R \tag{2}$$

where v_w is relative flow velocity and v_i is induced velocity, α is the angle between v_i and the direction from dl to the center of rotation,v_t denotes the velocity component in the tangential direction of dl. Hence, a resultant velocity can be determined through combining the two perpendicular velocity components, v_w and v_t.

Compatible with the direction of relative flow velocity v_w, a force triangle is constructed, as shown in Fig. 3. It is noteworthy that β, the angle between v_w and the direction from dl to the center of rotation, associates the velocity triangle with the force triangle. The relationship among those forces under consideration

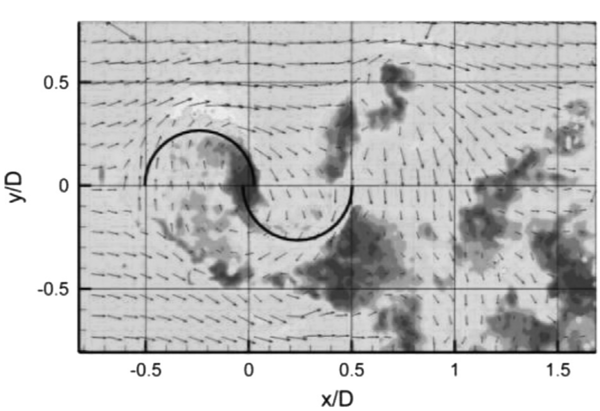


Fig. 4. Cross-sectional distribution of instantaneous velocity near a conventional Savonius wind rotor model.

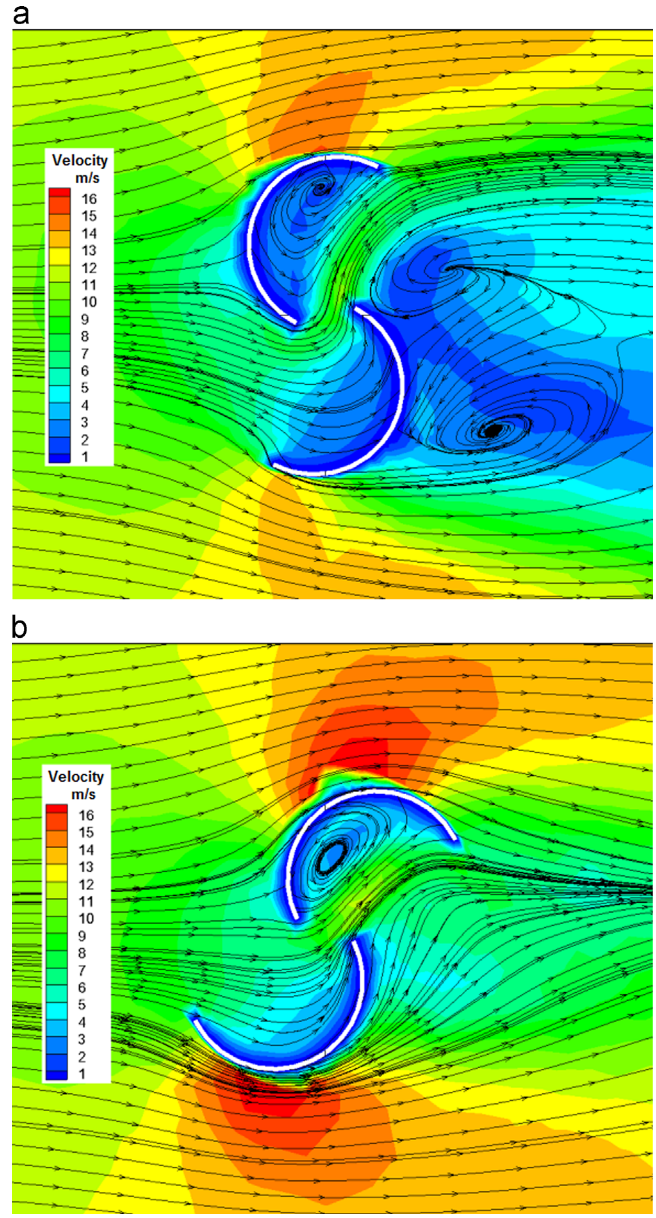


Fig. 5. Momentary distributions of velocity near a conventional Savonius wind rotor. The main stream flows from left to right. (a) Instance of maximum torque coefficient and (b) instance of minimum torque coefficient.

takes the form

$$\vec{F} = \vec{F}_W + \vec{F}_D \tag{3}$$

where $\vec{F}$ is resultant force, $\vec{F}_W$ and $\vec{F}_D$ are two component forces parallel and perpendicular to the relative flow velocity v_w, respectively.

Consequently, both resultant force and component forces acting on the advancing blade are obtained through the integration of dl along the physical boundary of the advancing blade. Difficulties residing in the above procedure can be readily perceived because the center of rotation does not coincide with the center of symmetry on the part of the advancing blade. Preferably, a specifically developed numerical code can be introduced to solve these equations approximately, as well as to organize relevant parameters in an efficient manner.

4. Consideration of flow patterns

4.1. Flow pattern around the conventional Savonius wind rotor

Albeit not well defined, flow patterns near the Savonius wind rotor contain the information that is more essential than that pertaining to the rotor itself. In a pioneering investigation, the flow pattern near a conventional Savonius wind rotor was visualized using the smoke-wire flow visualization technique [13]; at a given rotor height of 320 mm and an average flow velocity of 1.5 m/s, a nichrome wire of 0.1 mm in diameter was mounted at an upstream position 250 mm from the rotor axis, smoke was generated thereby. Alternatively, flow patterns near the Savonius wind rotor can be demonstrated in a quantitative manner, for instance, by flow velocity distribution. A recent study confirmed that the standard Pitot-static tube is effective in the velocity measurement near a stationary conventional Savonius wind rotor [14]. It is self-evident that flow patterns near stationary Savonius wind rotors are different from those near rotating Savonius wind rotors. Nevertheless, technical difficulties encountered in measuring or visualizing rotating flow fields are ubiquitous, and most of the difficulties implicate multidisciplinary knowledge [15]. In [16], a rotating transparent model of a conventional Savonius wind rotor was experimentally studied. A joint application of particle image velocimetry (PIV) and a synchronization system enabled the investigators to acquire instantaneous velocity near the rotor blades. And a cross-sectional distribution of instantaneous velocity is displayed in Fig. 4.

With such an experimental methodology, the results were claimed to approach the physical reality to a great extent. Even so, improvement is still sorely needed in measurement repeatability, image-processing capability and the uniformity of the light intensity distribution in the PIV window. To circumvent the difficulties caused by the rotation of the Savonius wind rotor, the frozen-rotor assumption was introduced. Under such an assumption, at each orientation angle between a rotor and upstream air flow, a corresponding flow field will be obtained. Through artificially changing the orientation angle, a string of flow fields will be obtained. And these sequentially arranged flow fields are supposed to be similar to the momentary flow fields arising with the rotation of the rotor.

As for the computational fluid dynamics (CFD) technique, which has penetrated deeply into the study of the Savonius wind rotor, two specific approaches were devised to tackle the interplay between a rotating rotor and ambient air flow. The first approach, exclusively feasible for steady simulation, converts transient flow into steady flow by virtue of the multiple reference frame (MRF) model. Such an approach is also known as the frozen-rotor approach. The other approach which is characterized by sliding meshes functions well in locating the time-varying interface between a rotating rotor and ambient air flow [17]. It has been corroborated that steady flow simulation yields overpredicted wind turbine efficiency, while unsteady flow simulation is more reliable in this connection. In addition, only unsteady flow simulation can be used to investigate the startup process of the Savonius wind rotor, because both shaft torque and static pressure vary violently in this startup process.

Two momentary cross-sectional distributions of velocity, which are extracted from a numerically obtained time-dependent velocity field surrounding a conventional Savonius wind rotor, are shown in Fig. 5(a) and (b), respectively. Meanwhile, momentary flow fields shown in Fig. 5(a) and (b) produce maximum and minimum torque coefficients, respectively. The situation indicated in Fig. 5(a) is advantageous in terms of boosting the anticlockwise rotation of the rotor. The two blades, namely advancing (lower) and returning (upper) blades, are approached by completely different flow structures, as determines the difference in the contribution to the increase of shaft torque between the two blades. Three large-scale vortices are prominent in Fig. 5(a). One vortex is trapped by the semi-circle area inside the returning blade, while the other two are situated immediately downstream of the advancing blade. The lower downstream vortex can be regarded as a typical flow structure in the wake region under consideration. The other downstream vortex, manifesting itself near the upper end of the advancing blade, is a product of the shear effect caused by the interaction between high-velocity gap flow and main stream. In addition, the gap flow is responsible for the formation of the vortex surrounded by the returning blade. From another perspective, the gap flow is connected with various aerodynamic losses, which explains the performance change of the Savonius wind rotor due to the removal of rotor shaft or the adjustment of overlap ratio. Furthermore, provided that a rotor shaft intrudes into the velocity field shown in Fig. 5(a), the gap flow pattern will undergo a considerable change [18].

Fig. 5(b) contains a relatively smooth flow field, which, however, renders the least assistance to the anticlockwise rotation of the rotor. The sole vortex that can be identified here is the vortex surrounded by the returning blade. The position of the vortex core is dependent upon the impingement of the gap flow on the returning blade, and this rationale also applies to the situation indicated in Fig. 5(a).

It is noteworthy that the largest vortex scale indicated in Fig. 5 is comparable to the radius of the rotor blade, and the flow field associated with the conventional Savonius wind rotor is featured by large-scale vortices. Furthermore, with the rotation of the rotor, formation, evolution and annihilation of large-scale vortices will occur periodically. And some relationship probably exists between the evolution of these vortices and the transient fluctuation of shaft torque, as has not been substantiated so far.

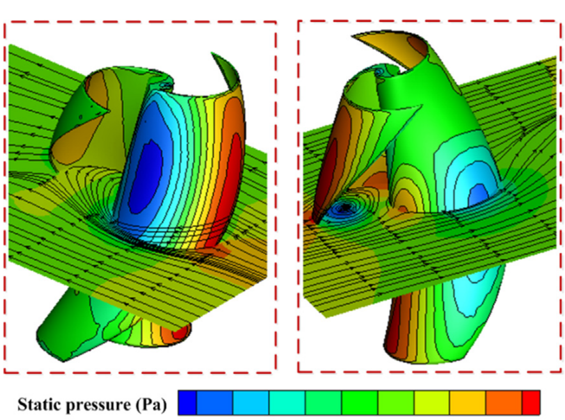


Fig. 6. A momentary flow pattern near a spiral Savonius wind rotor. (a) View 1 and (b) View 2.

4.2. Flow pattern around the spiral Savonius wind rotor

Relative to the two-dimensional flow field shown in Fig. 5, three-dimensional flow fields surrounding spiral Savonius wind rotors are considerably convoluted. A cross-sectional flow pattern extracted from such a three-dimensional flow field, in conjunction with static pressure distribution on blade surface, is viewed from two different angles, as shown in Fig. 6. Regardless of the direction of upstream air flow, as long as moving air enters the space surrounded by the two blades, it will provide momentum to the rotation of the rotor. In light of the geometric shape of the rotor shown in Fig. 6, it can be conjectured that flow patterns on different cross sections are distinctly various. Meanwhile, Fig. 6 merely indicates the flow

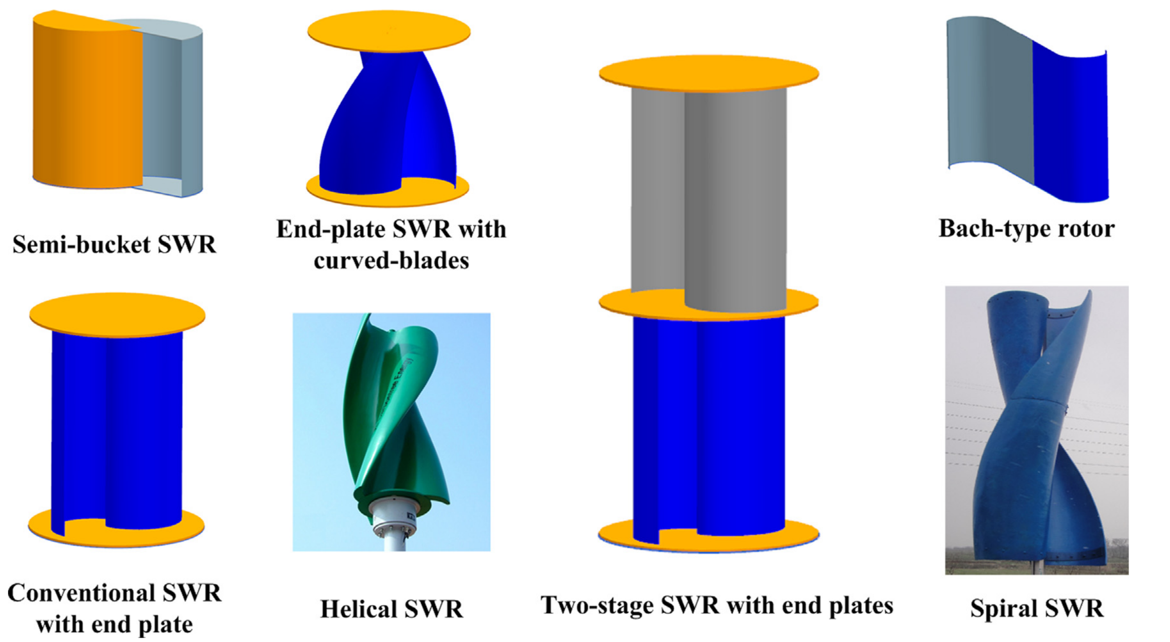


Fig. 7. Representative geometric shapes of Savonius wind rotors. Savonius wind rotor is abbreviated as SWR.

situation corresponding to a single moment; a variety of flow fields will be observed as the rotor rotates.

In recent years, numerical techniques have been overwhelmingly used in the study of curved-blade Savonius wind rotors [19–21]. As far as experimental practices are concerned, difficulties incurred by curved blades are evident. For instance, without specific development and calibration, general optical configurations cannot be used to probe into the local flow field shielded by a transparent curved blade with non-uniform surface curvatures. Additionally, during the design phase, owing to lack of more effective measures, empirical formulae have to be relied upon to determine geometric parameters of the curved-blade Savonius wind rotor.

4.3. Geometric characteristics of Savonius wind rotors

The coexistence of diverse geometric shapes with respect to Savonius wind rotors is a highlight in the field of wind turbines. Several Savonius wind rotors with different geometric shapes are exhibited in Fig. 7. These rotors can be classified into four types, namely straight-blade rotor, curved-blade rotor, multistage rotor and end-plate rotor. Intersection is inevitable among these four types and practical cases often cover two or more of the four types. One of the most primitive but significant applications of the Savonius wind rotor is to pump groundwater in some distant rural areas, as can be traced back to 1960s. Since such an application necessitates high shaft torque, the end-plate rotor and multistage rotor are preferable. According to an estimate based upon published treatises, the debut of the curved-blade Savonius wind rotor was in the late 1990s. Hitherto, a large body of literature has been dedicated to the topic of the curved-blade Savonius wind rotor. Besides, the Savonius wind rotor is involved in some combined rotors including the Darrieus-Savonius wind rotor, and the combined rotor is beyond the scope of this review [22].

As the most classical rotor type, the conventional Savonius wind rotor has geometrically different manifestations, which promote the diversity of consequent flow fields, and relevant flow investigations are still underway [23]. In this connection, many experimentally obtained conclusions cannot be generalized due to

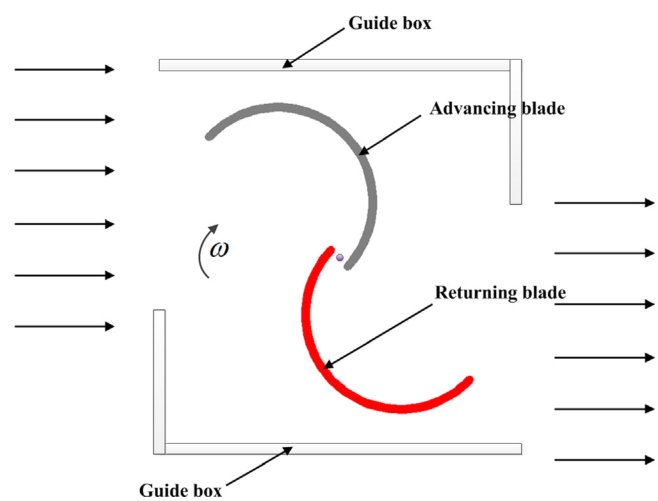


Fig. 8. Effective control of upstream air flow through guide-box tunnel.

lack of theoretical support. For instance, the test data indicate a dependence of shaft torque coefficient on dimensions of the central gap, but no quantitative relationship between geometric parameters of the central gap and performance parameters of the rotor is available [19]·[24]. Additionally, the motivation behind the structural development based upon the conventional Savonius wind rotor requires clear background. For instance, as shown in Fig. 7, a two-stage Savonius wind rotor, composed of two vertically superposed conventional Savonius wind rotors, can yield high shaft torque, but it cannot avoid the imperfection of the existing knowledge of conventional Savonius wind rotors [7]·[25].

In view of both mounting positions and appearance of end plates, a conventional Savonius wind rotor with two end plates is analogous to a Savonius wind rotor with two semi-bucket blades, as can be concluded from Fig. 7 [26]. In addition, end plates can also be used in collaboration with curved blades, as is also indicated in Fig. 7. It has been proven that the maximum power coefficient of an end-plate Savonius wind rotor attains 0.462 [27]. Another advantage of end plates is that they strengthen the overall structure of the rotor. As far as the end-plate Savonius wind rotor

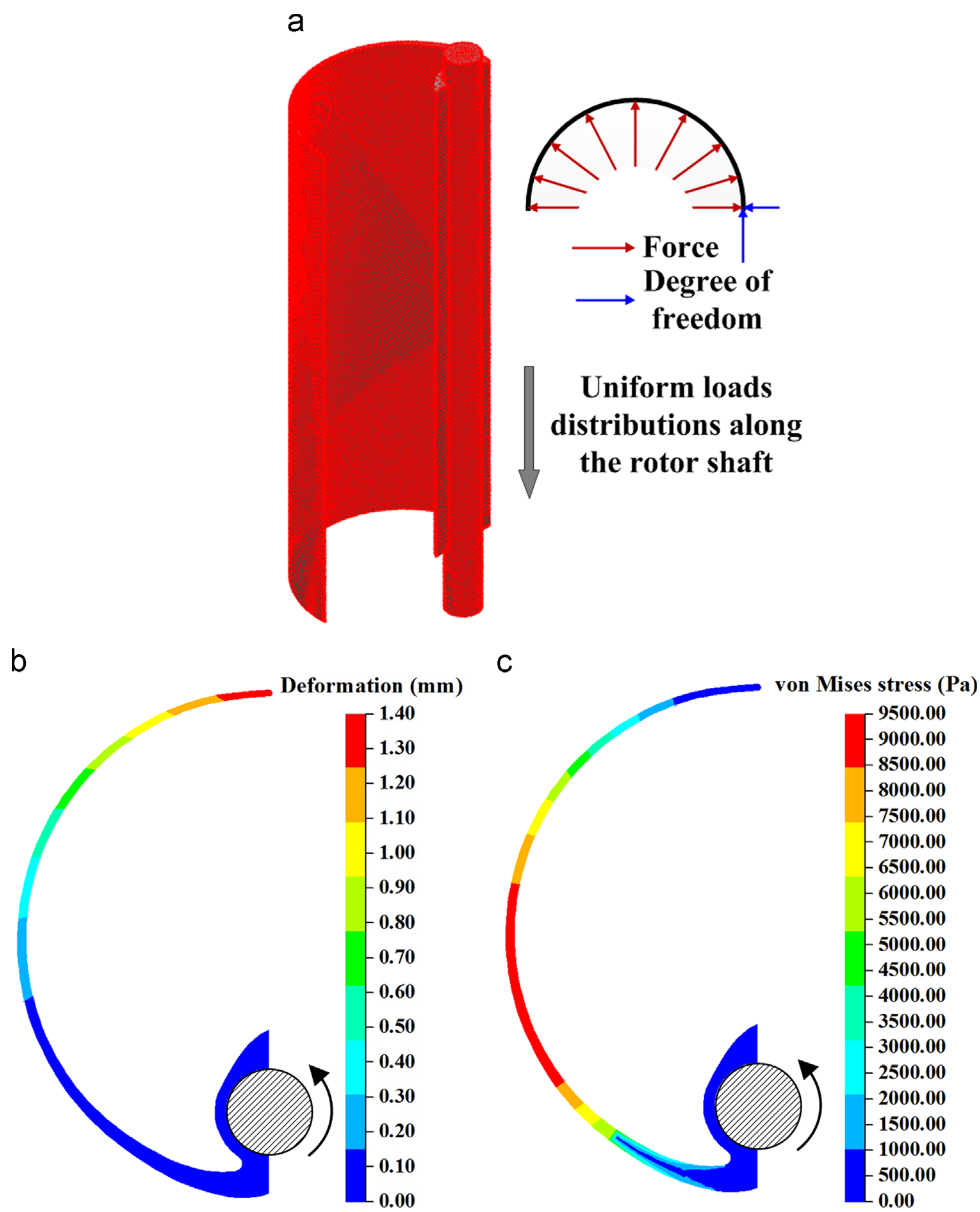


Fig. 9. Numerical calculation of deformation and internal stress distribution of a conventional Savonius wind rotor blade using finite element method. (a) Discretized solid domain and cross-sectional distribution of force loads, (b) deformation distribution and (c) von Mises stress distribution.

is concerned, structural attributes are of equivalent significance in comparison with flow characteristics.

The other straight-blade Savonius wind rotor shown in Fig. 7 is the Bach-type rotor. The presented cross section of the Bach-type rotor is characterized by a straight middle segment and a high curvature at blade tips. A numerical study has proven that the power coefficient of a well-designed Bach-type rotor is higher than that of a conventional Savonius wind rotor [28].

Savonius wind rotors armed with curved blades not only can adapt to air flows coming from all directions, but also can suppress shaft torque fluctuations [29]. These merits are particularly valuable for wind turbines with low tip-speed ratio. Furthermore, through an optimization of geometric parameters, the curved-blade Savonius wind rotor can acquire a maximum power coefficient comparable to that of the conventional Savonius wind rotor [4]·[30]. There are three most frequently used designations for curved blades, namely twisted blade, helical blade and spiral blade [31]. In this connection, both helical and spiral Savonius wind rotors are salient in Fig. 7 [3–4]. Superficially, no significant distinction is perceived among these three types of curved blades. Meanwhile, there is no clear geometric definition for the curved-blade Savonius wind rotor, and such a definition is not necessary either. Curved-blade Savonius wind rotors in service can be seen in USA, Japan and some other countries, and most of them are furnishing power to low power-consumption devices, as well as decorating local landscape.

Another group of Savonius wind rotors are equipped with various adjunct devices such as a shielding obstacle upstream of a returning blade, twin curtains adjusting upstream flow direction, and a conical concentrator before a three-stage rotor [32–36]. An adjunct device designated as the guide-box tunnel is shown in Fig. 8. With such a device, upstream air flow approaching a conventional Savonius wind rotor is clearly transformed. More specifically, the portion of upstream air that enters the guide-box tunnel drives the clockwise rotation of the advancing blade, while another portion of upstream air that would otherwise obstruct the clockwise rotation of the returning blade has no chance of contacting the returning blade. Although neither flow measurement nor flow simulation has been performed to flesh out such a description, the performance test data

obtained indicate unambiguously that the guide-box tunnel helps to improve the power coefficient of the conventional Savonius wind rotor [37].

5. Aerodynamic loads

5.1. Numerical treatment of internal stress distribution

The dynamic analysis of wind turbine structure has been given high priority on the part of large-scale horizontal-axis wind turbines. By contrast, similar work has rarely been reported concerning the Savonius wind turbine. Rated power output of most Savonius wind turbines in service is less than 2 kW, thus internal stress distribution of Savonius wind rotor blades is generally not deemed as an imperative issue. There was a reported case involving a Savonius wind turbine with a rated power output of 5 kW. The diameter and height of the rotor were 3500 mm and 7000 mm, respectively. And the blades were made from E-glass fiber. Under the optimal condition, tip-speed ratio of this wind rotor reached 1.0 at an air velocity of 10.5 m/s. To assess the operation stability of this wind rotor, the CFD technique and the finite element method (FEM) were jointly employed. Flow simulation was performed to obtain the static pressure distribution on blade surface, and this distribution served as a necessary boundary condition for the calculation of aerodynamic forces acting upon individual blades. Under the assumption of identical force magnitudes over the entire blade surface, both maximum and minimum von Mises stresses were calculated using a FEM static method [38]. Concerning this simulation process, divided opinions are being

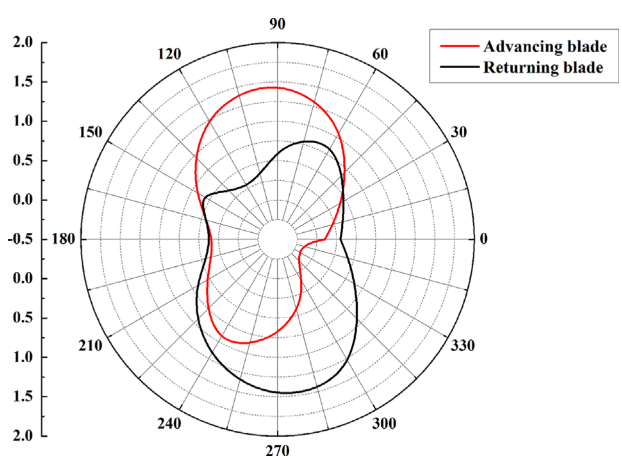


Fig. 10. Variation of resultant force coefficient associated with a conventional Savonius wind rotor rotating at a constant rotational speed.

concentrated on two subjects: one is the one-way coupling algorithm that only enables the unidirectional transmission of information from fluid to solid and the other is the influence of disparity of mesh density between solid and fluid domains on data communication via fluid–solid interface. As shown in Fig. 9(a), moderate-size three-dimensional FEM elements are utilized to discretize the solid domain occupied by one blade and one shaft, two vital components of a conventional Savonius wind rotor. Under an assumption of identical radial force magnitudes over the entire blade surface, deformation and von Mises stress are calculated and the results are shown in Fig. 9(b) and (c). The highest deformation occurs at the blade tip, and then the deformation decays consistently towards the blade root. Regarding von Mises stress, large values reign over a fairly broad cross-sectional segment, which is close to the blade root instead of the blade tip. It should be pointed out that these results are dependent to a great extent on rotor blade profile, as well as the predefined force loads acting on blade surface.

5.2. Transient force

Originating from flow field and affecting rotor blades, transient force is a parameter reflecting time-varying characteristics of both fluid part and solid part. Most importantly, transient force is immediately associated with shaft torque. A recent numerical study was dedicated to the calculation of the transient forces acting upon a conventional Savonius wind rotor [39]. A highlight in this study lies in that the rotational speed of the rotor is not predefined and rotation of the rotor around the rotor axis O_Z is governed by

$$J_{O_Z}\ddot{\theta} = (M_p + M_\tau + M_f) f_r \tag{4}$$

where J_{O_Z} is a component of the second-order rotor inertia tensor along O_Z, $\ddot{\theta}$ is angular acceleration, M_p is moment of pressure, M_τ is moment of viscous stresses, M_f is moment of external forces and f_r is a ramping factor, which is designed to restrict numerical oscillation during the initial phase of the simulation.

Therefore, the angular velocity of the rotor changes continually with the rotation of the rotor. Consequently, both the drag force in longitudinal direction and the lift force in lateral direction change accordingly. Time-dependent magnitudes of these two component forces set the stage for calculating transient resultant force. By contrast, many studies of conventional Savonius wind rotors calculate transient resultant force at a constant rotational speed of rotor, and the results obtained thereby are exemplified in Fig. 10, where the two closed curves representing resultant force coefficient are associated with advancing and returning blades, respectively. Only one single rotation period is counted in Fig. 10. To detail the calculation of force coefficients, the static pressure

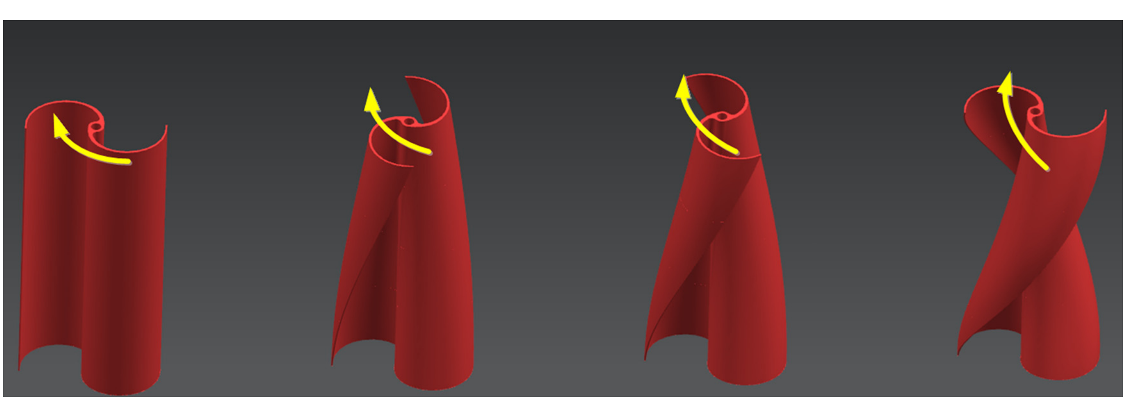


Fig. 11. Shaft torque characteristics of spiral Savonius wind rotors with various spiral angles. (a) $\psi = 0°$ (b) $\psi = 90°$ (c) $\psi = 120°$ and (d) $\psi = 180°$.

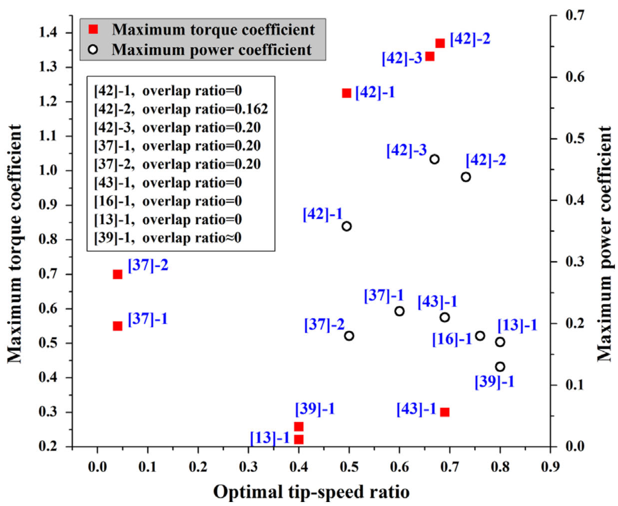


Fig. 12. Optimal values of tip-speed ratio of the Savonius wind rotor. The numbers in square brackets correspond to sequential numbers in the reference list. The numbers after hyphens represent different cases in the same study [43].

distribution along the physical boundary of a blade cross section is extracted from numerically obtained static pressure field, and then two perpendicular component forces acting upon the whole cross section are calculated through integrating scattered forces acting upon blade elements along the boundary. Consequently, with respect to a single blade or the whole rotor, both component force coefficients and resultant force coefficient are acquired.

Relative to numerical practices, the measurement of various forces acting upon the Savonius rotor blade requires stimulus. Small rotor scale and state of rotation are two primary factors that hamper the breakthrough in relevant measurement techniques. With available measurement apparatuses such as three-component force-balance meters, the resultant force acting upon the whole blade, instead of a force distribution, can be obtained. Additionally, to simplify the measurement procedure, the tested Savonius wind rotor blade is usually kept stationary. In this context, to mimic the condition of rotation, the relative orientation angle between the blade and upstream air flow is altered through two rotatable end plates on which the blade is fixed. An analogy between experimental results and corresponding physical reality is established thereby [40]. In this respect, a method used in the study of hydraulic turbines is instructive. The effectiveness of this method hinges upon two components; one is an array of strain gages stuck to curved-blade surface and the other is a slip ring designed to connect specialized rotational and stationary parts. A force distribution on the curved blade surface can be accomplished with this method. It is noteworthy that such a practice necessitates adequate sampling points and an elaborately fabricated test model.

5.3. Shaft torque characteristics of the curved-blade Savonius rotor

Shaft torque is a critical performance indicator for the Savonius wind rotor. Static torque meters can be used to measure shaft torque, circumventing inconveniences related to force measurement [41]. Alternatively, shaft torque can be calculated using CFD techniques [4]. As for the conventional Savonius wind rotor, the mechanism underlying the production of shaft torque has been well understood, and the direction of shaft torque is definite. By contrast, shaft torque characteristics of the curved-blade Savonius wind rotor are complicated in view of multidirectional forces acting on curved blades. Here, a spiral Savonius wind rotor is referred to as a representative of curved-blade Savonius wind rotors. Fig. 11 contains four spiral Savonius wind rotors with spiral angles of 0°, 90°, 120° and 180°, respectively. These four models are constructed based upon identical S-shape cross sections, and all rotor heights are equal too. Subject to identical upstream air flow conditions and rotational speed, the four rotors are distinctly different in resultant shaft torque. The $\psi=0°$ rotor is anticipated to gain the highest transient shaft torque among the four rotors, as is concluded through a comparison of the effective blade-air interaction areas associated with the four rotors, respectively. And the lowest level of shaft torque fluctuation with the rotation of the rotor is possessed by the $\psi=180°$ rotor, which maintains to the largest degree the circumferential structural balance of the whole rotor.

6. Tip-speed ratio

Tip-speed ratio is of great importance for all wind rotors. Many studies have indicated that there exists a correspondence between optimal value of tip-speed ratio and high-quality flow field, but further details are scarce. Although it has been observed that the flow pattern near a rotating Savonius wind rotor develops at a time scale which is exceedingly shorter than commonly used time intervals linking two successive angular positions of the rotating rotor, no pertinent quantitative explanation has been unfolded.

Several optimal values of tip-speed ratio, as well as the values of corresponding maximum torque and power coefficient, are shown in Fig. 12. Here, the optimal value of tip-speed ratio is defined as the tip-speed ratio at which maximum torque coefficient or maximum power coefficient is achieved. With respect to the same case, maximum torque coefficient and maximum power coefficient do not always meet the same tip-speed ratio, as is evidenced in Fig. 12. Moreover, although all rotors under consideration fall into the category of the Savonius wind rotor, discrepancy is obvious not only among those values of maximum torque coefficient but also among the values of maximum power coefficient. The highest coefficient of maximum torque arises in [42], where the semi-bucket Savonius wind rotor is concentrated on and the rotor with an overlap ratio of 0.162 bears a maximum torque coefficient of 1.3693, which is the largest among all values of maximum torque coefficient shown in Fig. 12. Meanwhile, the values of maximum power coefficient in [42] are also remarkable, and the rotor with an overlap ratio of 0.20 possesses a maximum power coefficient of 0.4668, which is superior to its counterparts shown in Fig. 12. It is noteworthy that all optimal values of tip-speed ratio shown in Fig. 12 range from 0.5 to 0.8, and the drag-dominating feature of the Savonius wind rotor manifests itself thereby.

As for the horizontal-axis wind rotor, tip-speed ratio has been effectively utilized to associate wake flow patterns with the performance of the rotor, and it has been substantiated that with the increase of tip-speed ratio, the vortices immediately downstream of the rotor blades tend to attenuate in terms of both vortex scale and vortex intensity [44]. Although the wake flow patterns related to the Savonius wind rotor are appreciably different with those seen downstream of the horizontal-axis wind rotor, it is equivalently significant to seek such a relationship to bridge the gap between typical flow characteristics and major performance parameters for the Savonius wind rotor. Such an exploration is anticipated to be carried out first for the conventional Savonius wind rotor, which is featured by typical large-scale flow structures and explicit torque-generation mechanisms.

7. Conclusions

This review underscores several subjects associated with both conventional and curved-blade Savonius wind rotors. In particular,

the flow-related subjects are elaborated on and discussed based upon those recent achievements. The following conclusions can be drawn from this review.

(1) The distinctiveness of the Savonius wind rotor is evidently reflected by flow patterns nurtured in the flow field surrounding Savonius wind rotor blades. Large-scale flow structures near the rotor blades are immediately associated with the rotation of the rotor blades. Three-dimensional flow patterns not just highlight curved-blade Savonius wind rotors but also cause difficulties for flow pattern description and rotor performance evaluation.
(2) The coexistence of geometrically different Savonius wind rotors is salient, and each Savonius wind rotor bears advantages as well as disadvantages. Adjunct devices play an important part in enhancing the operational capability of Savonius wind rotors. In some cases, structural attributes of Savonius wind rotors deserve a specific investigation performed with finite element method, and reasonable boundary conditions are necessitated as well.
(3) The employment of numerical techniques has proven to be fruitful in the study of the Savonius wind rotor. Both convoluted three-dimensional flow patterns and transient resultant forces acting upon Savonius wind rotor blades have been revealed with numerical techniques. And more significantly, the calculation of shaft torque can be realized using numerical techniques, which is based upon the basic relationship between shaft torque and aerodynamic forces.
(4) Two subjects are anticipated to be treated with special efforts. One is the development of experimental techniques for obtaining transient variations of both flow and rotor parameters with the rotation of the Savonius wind rotor, particularly the curved-blade Savonius wind rotor. The other one is the search of a robust connection between typical flow structures and optimal tip-speed ratio for conventional Savonius wind rotors.

Acknowledgments

This study is supported by the Jiangsu Overseas Research and Training Program for University Prominent Young and Middle-Aged Teachers and Presidents and the Priority Academic Program Development of Jiangsu Higher Education Institutions.

References

[1] Bhutta MMA, Hayat N, Farooq AU, Ali Z, Jamil SHR, Hussain Z. Vertical axis wind turbine–a review of various configurations and design techniques. Renew Sustain Energy Rev 2012;16:1926–39.
[2] Nakajima M, Iio S, Ikeda T. Performance of Savonius rotor for environmentally friendly hydraulic turbine. J Fluid Sci Technol 2008;3:420–9.
[3] Kang C, Zhang F, Yang MG, Mao XJ. Analysis of three-dimensional flow around a vertical-axis spiral wind rotor. Acta Energ Sol Sin 2011;32:1777–84.
[4] Kamoji MA, Kedare SB, Prabhu SV. Performance tests on helical Savonius rotors. Renew Energy 2009;34:521–9.
[5] Toja-Silva F, Colmenar-Santos A, Castro-Gil M. Urban wind energy exploitation systems: behaviour under multidirectional flow conditions—opportunities and challenges. Renew Sustain Energy Rev 2013;24:364–78.
[6] Menet J-L. A double-step Savonius rotor for local production of electricity: a design study. Renew Energy 2004;29:1843–62.
[7] Saha UK, Thotla S, Maity D. Optimum design configuration of Savonius rotor through wind tunnel experiments. J Wind Eng Ind Aerodyn 2008;96:1359–75.
[8] Vinay PV. Modified Savonius rotor for domestic power production. Int J Eng Sci Technol 2012;4(7):3256–60.
[9] Sabaeifard P, Razzaghi H, Forouzandeh A. Determination of vertical axis wind turbines optimal configuration through CFD simulations. In: International Conference on Future Environment and Energy, vol. 28; 2012. p. 109–13.
[10] Islam M, DS-K Ting, Fartaj A. Aerodynamic models for Darrieus-type straight-bladed vertical axis wind turbines. Renew Sustain Energy Rev 2008; 12:1087–109.
[11] Paraschivoiu I. Wind turbine design: with emphasis on darrieus concept. Presses Internationales Polytechnique. 2002.
[12] Biadgo AM, Simonovic A, Komarov D. Slobodan Stupar. Numerical and analytical investigation of vertical axis wind turbine. FME Trans 2013;41: 49–58.
[13] Fujisawa N, Gotoh F. Pressure measurements and flow visualization study of a Savonius rotor. J Wind Eng Ind Aerodyn 1992;39:51–60.
[14] Nasef MH, El-Askary WA, AbdEL-hamid AA, Gad HE. Evaluation of Savonius rotor performance: static and dynamic studies. J Wind Eng Ind Aerodyn 2013;123:1–11.
[15] McWilliam M, Johnson DA. Velocity measurement of flow around model vertical axis wind turbines. Int J Green Energy 2008;5:55–68.
[16] Dobrev I, Massouh F. CFD and PIV investigation of unsteady flow through Savonius wind turbine. Energy Proc. 2011;6:711–20.
[17] Jaohindy P, Ennamiri H, Garde F, Bastide A. Numerical investigation of airflow through a Savonius rotor. Wind Energy 2013. http://dx.doi.org/10.1002/we.1601.
[18] D'Alessandro V, Montelpare S, Ricci R, Secchiaroli A. Unsteady aerodynamics of a Savonius wind rotor: a new computational approach for the simulation of energy performance. Energy 2010;35:3349–63.
[19] Roy S, Saha UK. Review on the numerical investigations into the design and development of Savonius wind rotors. Renew Sustain Energy Rev 2013;24:73–83.
[20] Abbaszadeh M, Bagherzadeh F, Iravani M. A numerical investigation to study effects of a Savonius rotor's plate shape on its pptimum overlap ratio. In: Proceedings of the ASME 2012 Gas Turbine India Conference, paper no. GTINDIA2012-9655; 2012. p. 253–58.
[21] Kianifar A, Anbarsooz M. Blade curve influences on the performance of Savonius rotors: experimental and numerical. Proc Inst Mech Eng Part A: J Power Energy 2011;225:343–50.
[22] Gupta R, Sharma KK. Flow physics of a combined Darrieus–Savonius rotor using computational fluid dynamics (CFD). Int Res J Eng Sci Technol Innov 2012;1(1):1–13.
[23] Gupta R, Sharma KK. Flow physics of a three-bucket Savonius rotor using computational fluid dynamics (CFD). Int J Res Mech Eng Technol 2011;1 (1):46–51.
[24] Tong Z, Rempfer D. Numerical study of detailed flow field and performance of Savonius wind turbines. Renew Energy 2013;51:373–81.
[25] Al-Kayiem HH, Jin Ming G. Experimental investigation of S-rotors in open and bounded flows,. World Acad Sci Eng Technol 2011;60:144–9.
[26] Sheldahl RE, Feltz LV, Blackwell BF. Wind tunnel performance data for two- and three-bucket Savonius rotors. J Energy 1978;2:160–4.
[27] Deb B, Gupta R, Misra RD. Performance analysis of a helical Savonius rotor without shaft at 45° twist angle using CFD. J Urban Environ Eng 2013;7 (1):126–33.
[28] Kacprzak K, Liskiewicz G, Sobczak K. Numerical investigation of conventional and modified Savonius wind turbines. Renew Energy 2013;60:578–85.
[29] Kang C, Yang X, Wang YL. Turbulent flow characteristics and dynamics response of a vertical-axis spiral rotor. Energies 2013;6:2741–58.
[30] Damak A, Driss Z, Abid MS. Experimental investigation of helical Savonius rotor with a twist of 180°. Renew Energy 2013;52:136–42.
[31] Saha UK, Rajkumar MJ. On the performance analysis of Savonius rotor with twisted blades. Renew Energy 2006;31:1776–88.
[32] Mohamed MH, Janiga G, Pap E, Thévenin D. Optimization of Savonius turbines using an obstacle shielding the returning blade. Renew Energy 2010;35: 2618–26.
[33] Altan BD, Atılgan M. An experimental and numerical study on the improvement of the performance of Savonius wind rotor. Energy Convers Manag 2008;49:3425–32.
[34] Altan BD, Atılgan M, Özdamar A. An experimental study on improvement of a Savonius rotor performance with curtaining. Exp Therm Fluid Sci 2008;32:1673–8.
[35] Gogoi R, Mahanta RB, Das KK, Shah KK, Das G, Sharma KK. Experimental investigation of three-stage Savonius rotor with concentrator. Int J Mech Eng Res 2013;3(4):401–6.
[36] Chauvin AH, Belouaggadia N, Kamoun B. Influence of a deflector or a wall on Savonius rotor efficiency. J Env Sci Eng 2011;5:1294–6.
[37] Irabu K, Roy JN. Characteristics of wind power on Savonius rotor using a guide-box tunnel. Exp Therm Fluid Sci 2007;32:580–6.
[38] Widodo Chin WS, Sihombing ACH, Yuhazri MY. Design and analysis of 5 kW Savonius rotor blade. Global Eng Technol Rev 2012;2:1–8.
[39] Jaohindy P, McTavish S, Garde F, Bastide A. An analysis of the transient forces acting on Savonius rotors with different aspect ratios. Renew Energy 2013;55:286–95.
[40] Irabu K, Roy JN. Study of direct force measurement and characteristics on blades of Savonius rotor at static state. Exp Therm Fluid Sci 2011;35:653–9.
[41] Morshed KN, Rahman M, Molina G, Ahmed M. Wind tunnel testing and numerical simulation on aerodynamic performance of a three-bladed Savonius wind turbine. Int J Energy Environ Eng 2013;4:18.
[42] Gupta R, Biswas A, Sharma KK. Comparative study of a three-bucket Savonius rotor with a combined three-bucket Savonius-three-bladed Darrieus rotor. Renew Energy 2008;33:1974–81.
[43] Kamojia MA, Kedarea SB, Prabhub SV. Experimental investigations on single stage modified Savonius rotor. Appl Energy 2009;86:1064–73.
[44] Danmei H, Jie T, Chaohui D. PIV experimental study on the wake flow of horizontal-axis wind turbine model. Acta Energ Sol Sin 2007;28:200–6.